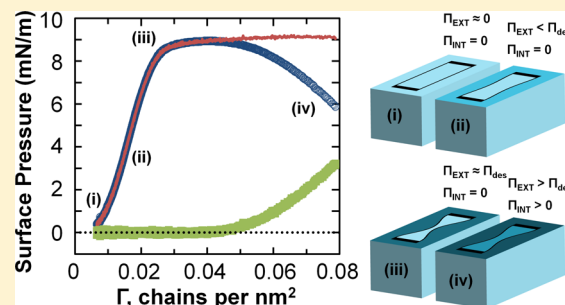


## Adsorption Energies of Poly(ethylene oxide)-Based Surfactants and Nanoparticles on an Air–Water Surface

Zachary A. Zell,<sup>†</sup> Lucio Isa,<sup>\*,‡,§</sup> Patrick Ilg,<sup>||</sup> L. Gary Leal,<sup>†</sup> and Todd M. Squires<sup>†</sup><sup>†</sup>Department of Chemical Engineering, University of California, Santa Barbara, Santa Barbara, California 93106-5080, United States<sup>‡</sup>Laboratory for Surface Science and Technology, Department of Materials, ETH Zurich, Wolfgang-Pauli-Strasse 10, 8093 Zurich, Switzerland<sup>§</sup>Laboratory for Interfaces, Soft matter and Assembly, Department of Materials, ETH Zurich, Wolfgang-Pauli-Strasse 10, 8093 Zurich, Switzerland<sup>||</sup>Polymer Physics, Department of Materials, ETH Zurich, Wolfgang-Pauli-Strasse 10, 8093 Zurich, Switzerland

## Supporting Information

**ABSTRACT:** The self-assembly of polymer-based surfactants and nanoparticles on fluid–fluid interfaces is central to many applications, including dispersion stabilization, creation of novel 2D materials, and surface patterning. Very often these processes involve compressing interfacial monolayers of particles or polymers to obtain a desired material microstructure. At high surface pressures, however, even highly interfacially active objects can desorb from the interface. Methods of directly measuring the energy which keeps the polymer or particles bound to the interface (adsorption/desorption energies) are therefore of high interest for these processes. Moreover, though a geometric description linking adsorption energy and wetting properties through the definition of a contact angle can be established for rigid nano- or microparticles, such a description breaks down for deformable or aggregating objects. Here, we demonstrate a technique to quantify desorption energies directly, by comparing surface pressure–density compression measurements using a Wilhelmy plate and a custom-microfabricated deflection tensiometer. We focus on poly(ethylene oxide)-based polymers and nanoparticles. For PEO-based homo- and copolymers, the adsorption energy of PEO chains scales linearly with molecular weight and can be tuned by changing the subphase composition. Moreover, the desorption surface pressure of PEO-stabilized nanoparticles corresponds to the saturation surface pressure for spontaneously adsorbed monolayers, yielding trapping energies of  $\sim 10^3 k_B T$ .



The self-assembly of polymer-based surfactants and nanoparticles on fluid–fluid interfaces is an important process which has been exploited for many applications, including dispersion stabilization and novel 2D material synthesis. Amphiphilic copolymers self-assemble into nanostructures via phase separation of chemically distinct units, both on a liquid substrate and in thin films, where the resulting nanostructure morphology can be controlled with the copolymer molecular weight, block mass percentage, and architecture.<sup>1–6</sup> Applications for these materials include high-resolution nanopatterned substrates, nanoporous membranes, lithographic masks, and other nanodevices.<sup>1–6</sup> Surface-active nanoparticles that adsorb to fluid–fluid interfaces enable fabrication of novel 2D materials with macroscopic structures that are used in membranes and capsules.<sup>7,8</sup> Moreover, inorganic cores can impart additional useful properties (e.g., magnetic, optical, and conductive) to nanoparticulate materials.<sup>9–11</sup>

Polymeric and nanoparticle surfactants preferentially adsorb to fluid–fluid interfaces whenever replacing a portion of the fluid–fluid interface with interfaces between the surfactant and the two fluids lowers the overall free energy of the system. The adsorption energy of the surface-active species gives a measure

of how effectively interfacial tension can be reduced and can be tuned by either modifications to the surface chemistry or bulk solution conditions. For micrometer-sized or submicrometer colloidal particles, the trapping energy is given approximately by the binding energy model,<sup>12</sup>  $\Delta E = -\pi R^2 \gamma_{12} (1 - \cos \theta_{eq})^2$ . The contact angle  $\theta_{eq}$  depends on the interfacial tensions between the liquids and solid particle,  $\gamma_1$  and  $\gamma_2$ , following Young's equation  $\cos \theta_{eq} = (\gamma_2 - \gamma_1) / \gamma_{12}$ , where  $\gamma_{12}$  is the interfacial tension between the fluids.

Recently, Du, Dinsmore, and co-workers measured the adsorption energy of polystyrene colloidal spheres directly by monitoring the effective interfacial tension reduction at an oil–water interface of a pendant drop due to the adsorbing particles and assuming a closed-packed monolayer.<sup>13</sup> The value of the adsorption energy compared well to predictions of the binding energy model obtained using the contact angle they measured. They used the same method to measure the binding energy of

Received: November 1, 2013

Revised: December 12, 2013

Published: December 16, 2013

rigid citrate-stabilized gold nanoparticles, whose measured  $\Delta E$  scaled with  $R^2$ , also in accordance with the binding energy model mentioned above.

However, recent experimental evidence suggests that assumptions of a well-defined contact angle and particle size/shape at the interface may break down for deformable objects, whereupon the continuum binding energy model would not be appropriate.<sup>14,15</sup> Additionally, such assumptions may break down if nanoparticles aggregate at the interface. In this case, the binding energy of a single particle is no longer sufficient to describe binding within a particle raft; instead, interactions between particles in the aggregates become relevant.<sup>16</sup>

Here, we present a general method to quantify the adsorption energy of surface-active, soluble materials. First, we demonstrate measurements of the adsorption energy of surface-active polystyrene-*b*-poly(ethylene oxide) (PS-PEO) block copolymers and poly(ethylene oxide) (PEO) homopolymers spread on air–water surfaces, varying both molecular weight and bulk solvent conditions. We then apply our technique to spread layers of iron oxide nanoparticles, each with a deformable poly(ethylene oxide) shell, focusing on how ligand molecular weight influences the adsorption energy of such core–shell nanoparticles.

## EXPERIMENTAL SECTION

**Polymers.** Water-soluble, yet highly surface-active poly(ethylene oxide) (PEO) homopolymers of varying molecular weight (0.6, 1.45, 3.35, 10, 100, and 300 kg/mol, Sigma-Aldrich; 6, 20, and 35 kg/mol, Fluka) were used as well as a polystyrene(28.8 kg/mol)-*b*-poly(ethylene oxide)(13.3 kg/mol) block copolymer of PDI 1.13, synthesized in the group of Dr. C. J. Hawker (UCSB).

**Nanoparticles.** Iron oxide–poly(ethylene oxide) (PEO) core–shell nanoparticles with an iron oxide core of mean diameter 8.4 nm were used in this study. Two types of particles were prepared using 2.5K and 5K linear poly(ethylene oxide) ligands (termed L2.5 and L5, respectively), using the preparation method described previously.<sup>17</sup> The “molecular weight” of a single nanoparticle was calculated from the mass of the core, the molecular weight of each polymer chain, and the grafting density<sup>17</sup> (1.67 and 1.40 MDa for L5 and L2.5, respectively).

**Monolayer Preparation.** All surfactants (homopolymer, block copolymer, and nanoparticles) were dispersed in chloroform and spread onto a high-purity water subphase (18 M $\Omega$ -cm, Milli-pore) within a Langmuir trough using a microsyringe. For the study on the effect of subphase composition, we prepared mixtures of high-purity water and ethylene glycol (BDH Chemicals). The surface density ( $\Gamma$ ) was determined from the mass of surfactant deposited, trough area, and surfactant molecular weight.

**Deflection Microtensiometer (MT).** We have previously described the microfabrication and operating principles of deflection microtensiometers (MT) in ref 18. The microtensiometer consists of an elongated rectangle, microfabricated using the photoresist SU-8 (2010 Series, Microchem) via contact photolithography, which is attached on one side to a grid to hold it in place (Figure 1c). Microtensiometer arms are long and slender so that they bend easily, whereas MT “end-caps” are made to be thicker to prevent bending and thus to impose effective “clamped” boundary conditions on the ends of the MT arm “beams.” The dimensions of the MTs used in this study are the following. MTs for PEO homopolymers: 3.41  $\times$  0.34 mm<sup>2</sup> MT internal area, 20  $\mu$ m MT arm width, 20  $\mu$ m MT arm height. Only the data in Figure 4 and the compression isotherm for PEO 0.6 kg/mol in Figure 5 have been recorded with a different MT, with dimensions 4.05  $\times$  0.34 mm<sup>2</sup> MT internal area, 20  $\mu$ m MT arm width, 20  $\mu$ m MT arm height. MTs for PEO nanoparticles: 4.05  $\times$  0.34 mm<sup>2</sup> MT internal area, 20  $\mu$ m MT arm width, 20  $\mu$ m MT arm height. MTs for PS-PEO block copolymers: 7.92  $\times$  0.98 mm<sup>2</sup> MT internal area, 70  $\mu$ m MT arm width, 12  $\mu$ m MT arm height.

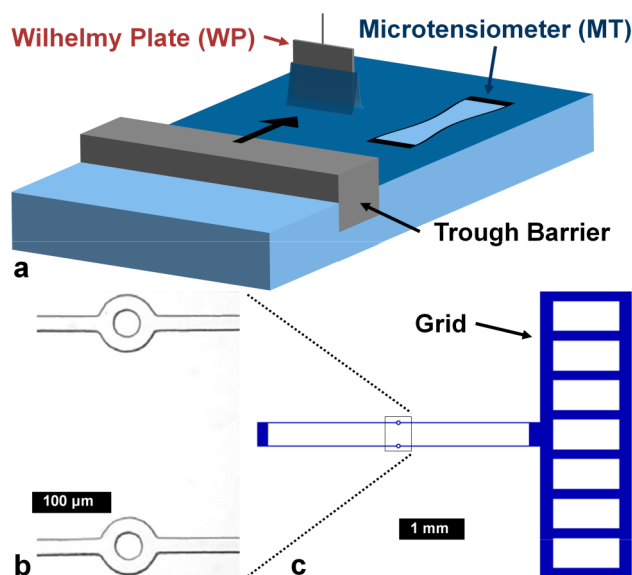


**Figure 1.** (a) Schematic representation of experimental setup of compression–surface pressure measurements: Langmuir trough, microtensiometer, and Wilhelmy plate. (b) Bright field image of microtensiometer center: circular markers enable real-time tracking of the deflection. (c) Top-down schematic of microtensiometer device with grid backbone used to hold it in place.

When placed at a liquid interface, the MT acts as a complete barrier that separates the internal interface from the external one. The inside of the microtensiometer is generally prepared to be surfactant-free, with “internal” surface pressure  $\Pi_{\text{INT}} = 0$ , whereas surfactant spread on the interface external to the MT exerts a nonzero “external” surface pressure  $\Pi_{\text{EXT}}$ . A surface pressure difference

$$\Delta\Pi_{\text{MT}} = \Pi_{\text{EXT}} - \Pi_{\text{INT}} \quad (1)$$

deflects the long, thin, MT arms. The measured deflection can be related directly to the instantaneous surface pressure difference  $\Delta\Pi_{\text{MT}}$  using elastic beam theory, from the geometry and elastic modulus of arms. When  $\Pi_{\text{INT}} = 0$ , the MT and WP give identical results.<sup>18</sup>

The microtensiometer is placed on a clean air–water surface of a Langmuir trough equipped with a Wilhelmy plate (Figure 1a). Wires affixed to the solid “grid” structure (Figure 1c) are used to maintain the MT in a fixed position for visualization and image analysis.

The microtensiometer is visualized in bright-field using a motorized zoom lens microscope (Navitar 6.5 $\times$ ) resting upon a motorized XYZ stage (ThorLabs). Images of the device center are acquired with a digital camera (Hitachi KP-F80SCL) and frame grabber (NI PCI-1428). The deflection of the MT arms is measured by tracking two circular markers located at their center (Figure 1b). A data acquisition device (NI PCIe-6353) measures the voltage output from the Wilhelmy plate system (Reigler & Kirstein) equipped with a filter paper plate. A custom LabVIEW code interfaced with the frame grabber and DAQ hardware is used to quantify the deflection of the MT beams (and thus surface pressure difference) in real time, while simultaneously controlling the barrier motion—generally compressing the surface at 4.5 cm<sup>2</sup>/min—as well as acquiring the surface pressure from the WP.

**Wilhelmy Plate Tensiometry of Nanoparticle Adsorption.** A Wilhelmy Plate (WP) tensiometer equipped with a roughened platinum plate (KSV 5000, Finland) was used to measure the surface pressure of aqueous NP suspensions at a flat air–water interface, which increased as NPs spontaneously adsorbed to the interface via diffusion through the bulk phase. The measurements were carried out by filling two identical containers with 5 mL of pure water and 10  $\mu$ M aqueous NP suspensions, respectively. The WP plate was first immersed in the pure water container to zero the pure air–water interfacial tension and then immersed in the aqueous NP suspension to the same immersion

height to measure the pressure due to NP adsorption. The whole zeroing process lasts less than a minute, but during this time some NPs already adsorb at the interface, which gives a nonzero surface pressure at the beginning of the curves in Figure 7c.

**Atomic Force Microscopy (AFM) Imaging.** To compare the morphology of the block copolymer monolayer to previous studies, we imaged transferred monolayers using AFM. First, Langmuir–Schaefer deposition was used to transfer the block copolymer monolayer to a solid substrate. A mica surface (S&J Trading Inc.) is placed directly below the air–water surface. After spreading 8–10  $\mu\text{L}$  of a chloroform solution containing PS–PEO, the surface is compressed to the desired surface pressure. A syringe pump is used to remove water from behind the barrier at 10 mL/min, which slowly lowers the level of the interface and transfers the monolayer to the mica substrate. The mica substrate with the deposited monolayer is then imaged in AFM tapping mode (MMAFM-2, Digital Instruments) with a cantilever tip (Asylum Research, AC160TS).

## RESULTS AND DISCUSSION

To measure adsorption energies of surface-active species, we compare surface pressure ( $\Pi$ )–density ( $\Gamma$ ) compression measurements taken simultaneously in a Langmuir trough using a Wilhelmy plate tensiometer (WP)—which measures the surface pressure of a liquid surface ( $\Pi_{\text{WP}}$ )—and a custom-built, deflection microtensiometer (MT)<sup>18</sup> (Figure 1), as described above.

**Polymeric Surfactants.** Figure 2a shows quantitative agreement between the microtensiometer and Wilhelmy plate in the measured  $\Pi$ – $\Gamma$  isotherm of the block copolymer PS–PEO, spread at an air–water surface, over the entire

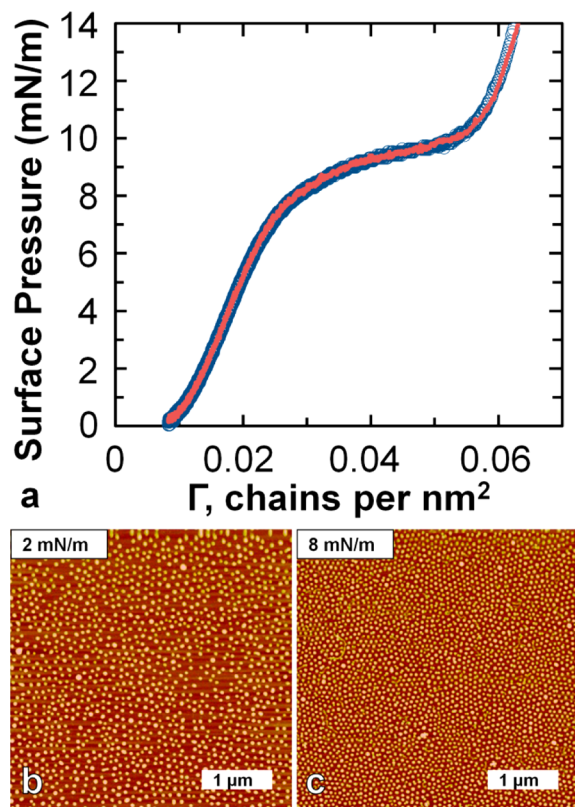


**Figure 2.** (a)  $\Pi$ – $\Gamma$  compression isotherm of block copolymer PS–PEO: MT (open blue circles) and WP (red line) agree over entire concentration range; AFM images of deposited block copolymer monolayer at (b) 2 mN/m and (c) 8 mN/m show formation of nanosized surface aggregates.

concentration range. The isotherm is similar to previously reported PS–PEO isotherms:<sup>19–21</sup> at low concentrations, the surface pressure increases gradually as the film is compressed, exhibits a pseudo-first-order plateau at intermediate pressures ( $\sim 8$ – $10$  mN/m), and then increases sharply with concentration. AFM imaging of the monolayer after Langmuir–Schaefer deposition (Figure 2b,c) reveals a microstructure of self-assembled nanodots, similar to those observed with block copolymers containing 30 wt % PEO.<sup>22–25</sup> These structures form due to aggregation of the hydrophobic polystyrene block and consist of a PS-rich core stabilized by the PEO block underneath and in the corona, and the sharp increase in  $\Pi$  indicates repulsion between the aggregate cores. The highly insoluble PS core anchors the aggregates to the surface, resulting in behavior typical of an insoluble monolayer.

Similar features are seen with 10K PEO homopolymer chains at low surface pressures, but significant differences between  $\Delta\Pi_{\text{MT}}$  and  $\Pi_{\text{WP}}$  appear at higher  $\Pi$  (Figure 3a). At low surface

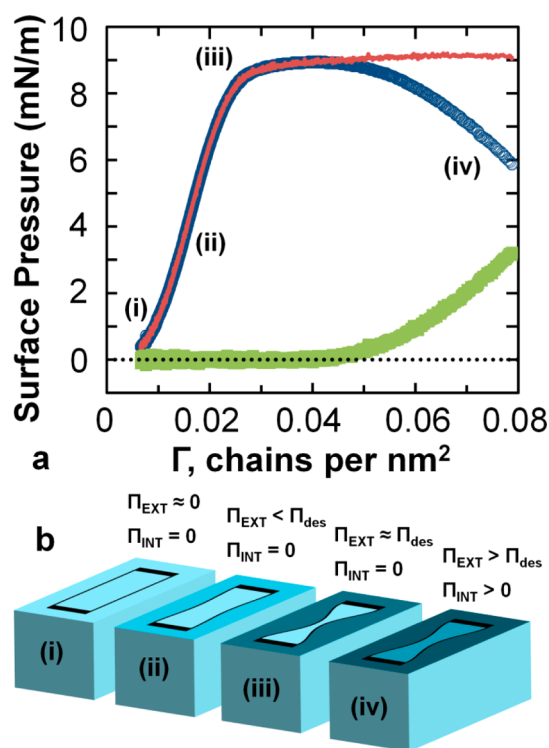


**Figure 3.** (a)  $\Pi$ – $\Gamma$  compression measurement of homopolymer PEO (10 kg/mol): MT (open blue circles) and WP (red line) agree at low pressures (i–iii) and concentrations until deviating near 9 mN/m. The surface pressure on the interior area of the MT (green squares, obtained by subtracting the MT signal from the WP signal) becomes nonzero upon continued compression, indicating readsorption of PEO chains on the inside (iv). (b) Schematic representation of MT under (i–iii) compression and (iv) desorption/readsorption process. Shaded areas indicate adsorbed PEO layer.

concentrations, the MT and WP isotherms agree quantitatively, as in Figure 2a for PS–PEO monolayers. Above  $\Gamma \approx 0.04$ – $0.05$  chains/ $\text{nm}^2$ , however,  $\Delta\Pi_{\text{MT}}$  deviates from  $\Pi_{\text{WP}}$ . While  $\Pi_{\text{WP}}$  plateaus at 9 mN/m,  $\Delta\Pi_{\text{MT}}$  decreases as  $\Gamma$  increases.

The plateau in surface pressure at high surface densities has typically been attributed to monolayer collapse and solubilization of PEO into the water subphase.<sup>26–33</sup> Partial desorption of PEO would not explain the discrepancy between  $\Delta\Pi_{\text{MT}}$  and  $\Pi_{\text{WP}}$ , since segment desorption would affect  $\Delta\Pi_{\text{MT}}$  and  $\Pi_{\text{WP}}$  in

the same way. Instead, our data at high surface concentration suggest that entire PEO chains detach, diffuse through the bulk underneath the MT arms, and reabsorb onto the initially clean internal MT surface, increasing  $\Pi_{\text{INT}}$  and thus decreasing  $\Delta\Pi_{\text{MT}}$  via eq 1.

Figure 4a provides further confirmation of this mechanism. A 10K PEO monolayer was compressed at 4.5  $\text{cm}^2/\text{min}$  for

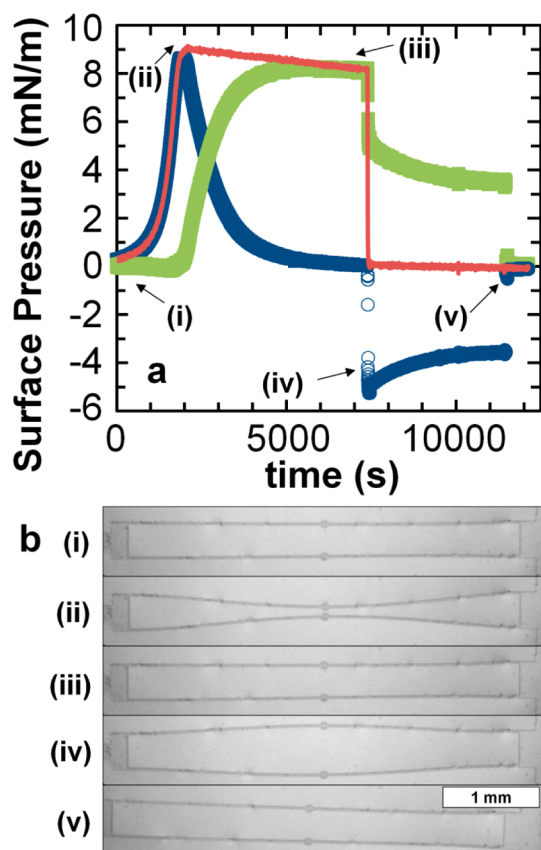


**Figure 4.** (a) External and internal surface pressures and surface pressure difference for compressed monolayer of 10K PEO plotted against time, with  $\Delta\Pi_{\text{MT}}$  (open blue circles),  $\Pi_{\text{WP}}$  (red line), and  $\Pi_{\text{INT}} = \Pi_{\text{WP}} - \Delta\Pi_{\text{MT}}$  (green squares) as in Figure 3. Compression starts at (i), increasing  $\Pi_{\text{EXT}}$ .  $\Delta\Pi_{\text{MT}}$  reaches a maximum and then decreases near the end of the compression cycle at (ii) as PEO chains desorb from the external interface and reabsorb to the internal section (iii). Once reabsorption completes ( $\Delta\Pi_{\text{MT}} \approx 0$ , iii), the barrier is retracted to increase external surface area, reducing  $\Pi_{\text{EXT}}$  approximately to 0. The negative pressure difference ( $\Delta\Pi_{\text{MT}} < 0$ ) indicates polymer is adsorbed on the internal surface, swelling the MT arms (iv). Upon aspirating the internal surface, the pressure difference  $\Delta\Pi_{\text{MT}}$  returns to zero (v). (b) Bright-field images of microtensimeter at stages (i–v) described in (a), for an analogous experiment with 3.35K PEO.

2100 s to  $\Delta\Pi_{\text{MT}} \sim 8.5$  mN/m and then held at fixed area. In the time that followed, the surface pressure difference  $\Delta\Pi_{\text{MT}}$  measured by the microtensimeter decreased steadily, essentially reaching zero after approximately 1 h. Once  $\Delta\Pi_{\text{MT}}$  reached zero, the barrier was retracted to increase the external surface area, rapidly decreasing  $\Pi_{\text{EXT}}$ . The MT arms swelled outward, indicating a negative  $\Delta\Pi_{\text{MT}}$  and thus  $\Pi_{\text{EXT}} < \Pi_{\text{INT}}$ , confirming that surfactant had indeed reabsorbed onto the internal surface. The pressure difference remained negative until the internal surface of the MT was aspirated (at  $t \approx$

11 500 s), returning  $\Pi_{\text{INT}}$  and thus  $\Delta\Pi_{\text{MT}}$  to 0, and restoring the original MT shape (Figure 4b).

Desorbing a single chain from a densely populated surface opens up an area  $\Delta A = 1/\Gamma$  of “clean” interface into which other adsorbed chains can spread and relax. The free energy of the interfacial layer is then reduced by an amount  $\Delta E = -\int \Pi \, dA$ , or approximately  $-\Pi\Delta A \sim -\Pi/\Gamma$  for small chain areas. At a critical desorption pressure ( $\Pi_{\text{des}}$ ) and surface density ( $\Gamma_{\text{des}}$ ), the work  $\Delta E_{\text{des}}$  required to desorb one chain is precisely compensated by the free energy gained by expansion of the remaining adsorbed chains and is given by

$$\Delta E_{\text{des}} = \frac{\Pi_{\text{des}}}{\Gamma_{\text{des}}} \quad (2)$$

The desorption energy  $\Delta E_{\text{des}}$  can thus be determined by measuring the critical values  $\Pi_{\text{des}}$  and  $\Gamma_{\text{des}}$  where desorption begins to occur.

Equation 2 relates the equilibrium desorption energy to a maximum steady surface pressure and concentration, above which chain desorption is thermodynamically favored. The practical measurement of  $\Delta E_{\text{des}}$  however, can be limited by two dynamic processes. First, the kinetics of desorption and adsorption may itself be prohibitively slow, particularly when  $\Delta E_{\text{des}} \gg k_{\text{B}}T$ . Second, the desorbed material must be transported to the “internal” MT interface and reabsorb. If the mass transport is primarily diffusive, equilibration past a barrier of length  $L$  requires a time scale  $L^2/D$ . Given the dimensions of the microtensimeter arms (see Experimental Section), and diffusivities ranging from  $3.6 \times 10^{-10} \text{ cm}^2/\text{s}$  for the smallest homopolymers to  $1.1 \times 10^{-11} \text{ cm}^2/\text{s}$  for the largest ones,<sup>34</sup> mass transport times range from 10 to 330 s. We cannot exclude the presence of convection in the experiments, which will reduce the time lag in a way that cannot be controlled in our setup. We therefore assign an upper bound for  $\Pi_{\text{des}}$  and  $\Gamma_{\text{des}}$  by the point where the internal  $\Pi_{\text{INT}}$  exceeds the collective sensitivity of the MT/WP measurement, which is 0.2 mN/m, and note that one source of experimental uncertainties is given by the time for mass transport relative to the compression rate. Desorption of 10K PEO starts at  $\Pi_{\text{des}} = 9$  mN/m and  $\Gamma_{\text{des}} = 0.048$  chain/ $\text{nm}^2$ , from which  $\Delta E_{\text{des}} \approx 46 k_{\text{B}}T/\text{chain}$ . While we have assumed no barriers to adsorption on the (clean) internal surface to the MT, such kinetic barriers could exist for other surfactants and would introduce a further delay in the detected desorption.

The compression measurements in Figure 5a show that both the surface pressure and concentration at the desorption transition depend upon the PEO molecular weight (Figure 5b,c). We find that  $\Pi_{\text{des}}$  follows a similar trend with  $M_{\text{W}}$  as previously reported collapse pressures,<sup>29,30,33</sup> becoming nearly independent of  $M_{\text{W}}$  above  $O(10 \text{ kg/mol})$ . Higher molecular weight PEO is more likely to remain anchored to the surface until higher surface pressures and higher monomeric surface densities<sup>33</sup> are reached, as it can be seen in Figure 5b,c. The adsorption energy per chain in Figure 5d scales linearly with molecular weight or number of segments, suggesting that the chain is strongly adsorbed to the interface. Furthermore, the scaling indicates a desorption energy that varies in proportion with the physical area occupied by the polymer chain at the interface (itself a linear function of the number of monomers  $N$ ).<sup>35,36</sup> Assuming  $\Delta E_{\text{chain}} = N\Delta E_{\text{monomer}}$ , we find an adsorption energy of approximately  $0.15 k_{\text{B}}T$  per monomer.

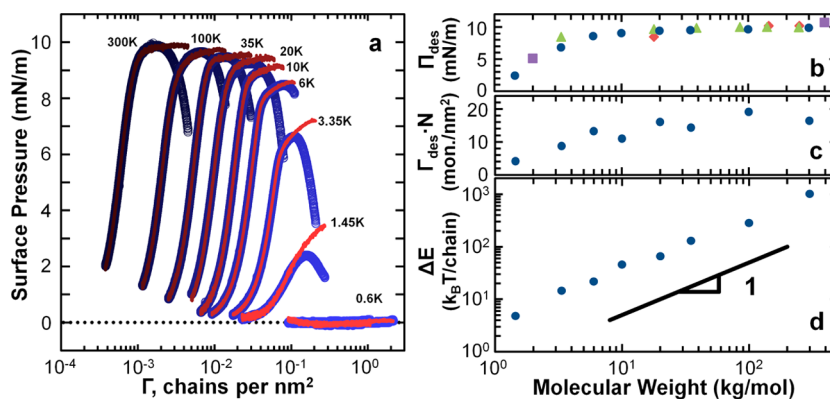


**Figure 5.** (a)  $\Pi$ – $\Gamma$  compression measurements of homopolymer PEO with varying molecular weight (0.6–300 kg/mol). MT (open blue circles) and WP (red lines) agree at low pressures and concentrations and then deviate at a  $M_W$ -dependent surface pressure (b) and surface density (c). The measured surface pressure at desorption (blue circles) and its dependence on  $M_W$  coincide well with previously reported collapse pressures of PEO homopolymer monolayers [green triangles, ref 29; red diamonds, ref 30; purple squares, ref 33]. (d) The measured adsorption energy scales linearly with the molecular weight, indicating a chain desorption energy  $\Delta E_{\text{chain}} = N\Delta E_{\text{monomer}}$ , where the desorption energy per monomer  $\Delta E_{\text{monomer}} \approx 0.15 k_B T$ .

Lastly, the lack of any measurable surface pressure for a 0.6 kg/mol PEO sample spread at a similar initial surface density of EO monomers (Figure 5a) suggests a lack of surface activity of these chains. This may not be surprising, considering that our assumed value of  $0.15 k_B T$  per monomer would imply only  $2 k_B T$  total adsorption energy for each chain.

The EO monomer adsorption energy has previously been estimated from surface pressure/area isotherms of PS–PEO block copolymers.<sup>19,21</sup> The appearance of a pseudoplateau at a surface pressure of approximately 10 mN/m is linked to the onset of solubilization of PEO segments and the transition between a fully adsorbed copolymer layer to a configuration where the PS blocks stay anchored at the interface and PEO chains form a brush in the water subphase. Bijsterbosch and co-workers<sup>19</sup> estimated an effective adsorption energy of  $0.4 k_B T$  per monomer using scaling estimates of the surface density of EO monomers. Faure and co-workers<sup>21</sup> found optimal agreement between their measured isotherms and ones obtained from single chain mean-field calculations when their adsorption energy parameter was chosen to be about  $1 k_B T$  per monomer. Given the smooth transition to the pseudoplateau in the experimental data (as opposed to a sharp transition in the SCMF predictions), it is difficult to estimate the onset of segment desorption with high accuracy. Moreover, the presence of the PS anchoring blocks may influence the density profile of desorbed EO segments close to the interface. Given the sharp experimental signature of our method, and the cleaner physical measurable (i.e., complete desorption of simple PEO homopolymer segments), our measurement should be free of these additional complications.

Subphase composition also affects PEO desorption energy (Figure 6). Figure 6a shows a gradual shift of 10K PEO isotherms to lower surface pressures, as the fraction of ethylene glycol (EG) in the subphase is increased (from 0 to 1, 4, 8, and 16 wt %). The reduction in the measured surface pressure at desorption ( $\Pi_{\text{des},0} - \Pi_{\text{des}}$ ) varies linearly with the reduction in the subphase surface tension ( $\gamma_0 - \gamma$ ) caused by the added ethylene glycol<sup>37</sup> (Figure 6c). The addition of ethylene glycol may also change  $\Gamma_{\text{des}}$  for a given PEO  $M_W$ ; however, variations appear too small to be measured accurately (Figure 6b). The reduction in adsorption energy ( $\Delta E_0 - \Delta E$ ), calculated from the surface pressure reduction at an average  $\Gamma_{\text{des}}$  of 0.048

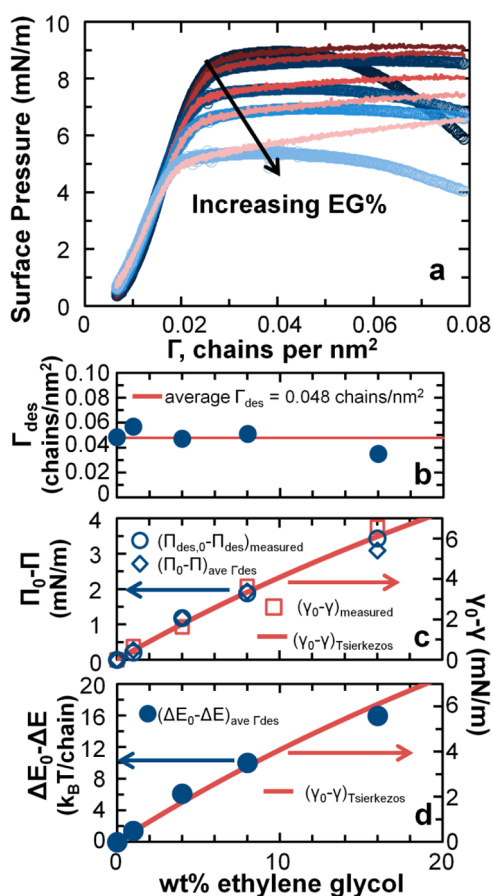


**Figure 6.** (a) Adding monomeric ethylene glycol to the subphase (from 0 to 1, 4, 8, and 16 wt %) shifts  $\Pi$ – $\Gamma$  compression curves of 10K homopolymer PEO to lower pressures. MT (open blue circles) and WP (red lines) agree at low pressures and concentrations, yet deviate at an EG%-dependent surface pressure. While only small variations are observed in the measured surface concentration at desorption (b), the reduction in the surface pressure at desorption is proportional to the reduction in subphase surface tension due to adding ethylene glycol. (c) Reduction in the surface pressure at desorption is proportional to the reduction in subphase surface tension due to adding ethylene glycol. (d) Reduction in PEO adsorption energy (computed using average  $\Gamma_{\text{des}} \sim 0.048$  chain/ $\text{nm}^2$ ) increases with the amount of EG in the subphase and also shows a linear variation with the reduction in subphase surface tension.

chain/nm<sup>2</sup>, also shows a linear variation with the subphase surface tension reduction (Figure 6d). This strong correlation with surface tension indicates that the decrease in polymer adsorption energy reflects the competition between adsorption of polymeric and monomeric ethylene glycol. Monomeric ethylene glycol reduces surface tension as it adsorbs, some of which must be displaced for PEO to adsorb, at a free energy cost that reduces the net free energy of adsorption for a PEO chain. Conversely, desorption of a PEO chain, which would require  $N\Delta E_{\text{monomer}}$  on a clean interface, is partially compensated by the re-adsorption of EG monomers, reducing the desorption energy.

**Nanoparticle Surfactants.** Having built a consistent picture of the PEO adsorption/desorption energy at aqueous interfaces, we turn to PEO-coated iron oxide nanoparticles spread at air–water surfaces. Several techniques have been previously employed to detect desorption of nanoparticles from fluid interfaces. Garbin and co-workers<sup>38</sup> mechanically forced gold nanoparticles to desorb from the interface of a pendant oil–water drop, detected the desorbed particles optically, and used eq 2 to determine  $\Delta E_{\text{des}}$ , with results that were similar to the adsorption measurements of Du et al.<sup>13</sup> Stefaniu and co-workers<sup>39</sup> detected the desorption and re-adsorption of copolymer-coated iron oxide nanoparticles, similar to the ones presented here, from air–water interfaces. Using two Wilhelmy plates, they measured the surface pressure on both sides of a Langmuir trough barrier and detected the re-adsorption of desorbed particles onto the (initially clean) surface behind the barrier, akin to the  $\Pi_{\text{INT}}$  measurements made by our MT. Additionally, they transferred the interface behind the barrier onto a solid surface and used atomic force microscopy to verify nanoparticle re-adsorption.

Results from the WP/MT technique described here are consistent with these earlier techniques, with several advantages. The microtensiometer can detect desorption/re-adsorption (and thus measure  $\Delta E_{\text{des}}$ ) for surfactants that cannot be detected optically. Furthermore, the MT introduces a significantly lower barrier to mass transport: desorbed particles or surfactants must diffuse only tens of micrometers, rather than centimeters, to traverse the barrier, thereby reducing measurement delays and uncertainties.

Figure 7a,b shows the characteristic agreement between MT and WP at low nanoparticle surface concentrations, followed by deviations at higher pressures and concentrations. As with the PEO polymer surfactants, we interpret these deviations in terms of nanoparticle desorption and re-adsorption inside the MT. To confirm re-adsorption of the L5 nanoparticles to the internal surface, we expanded the external surface area at  $\sim 3750$  s in Figure 7a, decreasing the external surface pressure rapidly, leading to a negative measured  $\Delta\Pi_{\text{MT}}$  (positive  $\Pi_{\text{INT}}$ ). Following the external expansion,  $\Pi_{\text{INT}}$  remains stable until the internal interface is aspirated at  $\sim 4100$  s.

Uncertainties in the measured values of  $\Delta E_{\text{des}}$  arise due to the finite time required for desorption/re-adsorption processes to occur, whether due to finite desorption kinetics or mass transport delays while desorbed NPs diffuse under MT arms. Figure 8 shows stepped-compression experiments designed to measure NP adsorption energy more accurately by minimizing the impact of these delays upon the measured  $\Pi_{\text{des}}$ . In stepped-compression experiments, the concentration is increased slowly, in discrete increments of  $\Delta\Gamma/\Gamma_0 = 0.2$ , each followed with a 5 min period (which is longer than  $L^2/D$  for the nanoparticles) where the area was held constant to allow for internal relaxation

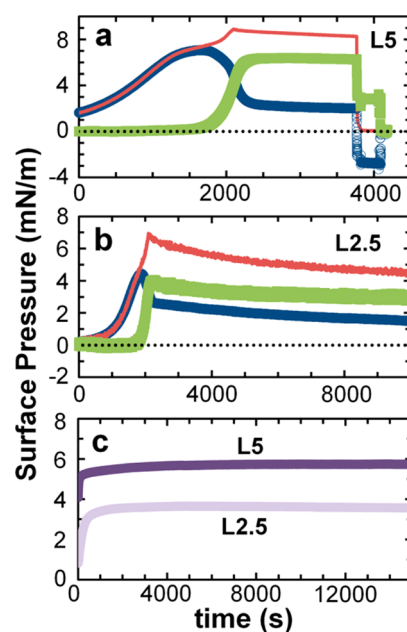


**Figure 7.** Surface pressures ( $\Pi$ ) plotted as a function of time for iron oxide nanoparticles with varying PEG ligands: (a) L5 and (b) L2.5. In each case, the monolayer is compressed at a uniform rate until  $\sim 2100$  s, and then compression stops. Measurements using the MT (open blue circles) and WP (red line) agree at low pressures and then deviate at higher surface pressures. As with PEO homopolymers (Figure 4), this deviation indicates a positive surface pressure  $\Pi_{\text{INT}}$  (green squares) on the internal interface of the MT caused by nanoparticles that had desorbed and re-adsorbed internal to the MT. To confirm the hypothesized re-adsorption, the external interface is expanded at  $\sim 3750$  s in (a), lowering the external pressure to approximately zero. The internal pressure remains nonzero until aspiration at  $\sim 4100$  s. (c) Dynamic surface pressure of spontaneous NP adsorption from an aqueous NP solution, measured using a Wilhelmy plate. The equilibrium saturation pressures agree with the long-time surface pressure values of the internal surface of the MT due to re-adsorbing nanoparticles.

of the monolayer. The  $\Pi_{\text{des}}$  values obtained from stepped-compression— $3.9$  mN/m for L2.5 and  $5.7$  mN/m for L5 (Table 1)—are somewhat lower than those obtained in continuous compression ( $4.4$  mN/m for L2.5 and  $7.2$  mN/m for L5), most likely because potential delays due to mass transport or desorption kinetics were minimized by the equilibration times designed into the stepped compression experiments. Values from stepped-compression experiments agree with the saturation surface pressures achieved during spontaneous adsorption from a  $10 \mu\text{M}$  bulk aqueous solution, measured with a stand-alone Wilhelmy plate tensiometer (Figure 7c,  $\Pi_{\text{sat,soln(WP)}}$ :  $3.6$  mN/m for L2.5 and  $5.7$  mN/m for L5). Moreover, the saturation surface pressures from spontaneous adsorption are comparable to the long-time internal surface pressures measured with the MT/WP technique ( $\Pi_{\text{sat,INT(MT/WP)}}$ :  $3.0$  mN/m for L2.5 and  $6.4$  mN/m for L5 in Figure 7a,b). Measured adsorption energies for the PEO-coated nanoparticles, listed in Table 1, are of order  $1000 k_{\text{B}}T$ , similar to values calculated previously for similarly sized nanoparticles at decane–water interfaces.<sup>14</sup> We will compare below our results to a simple model, but we already note that as expected, the largest nanoparticles, with SK linear ligands, have higher adsorption energy.

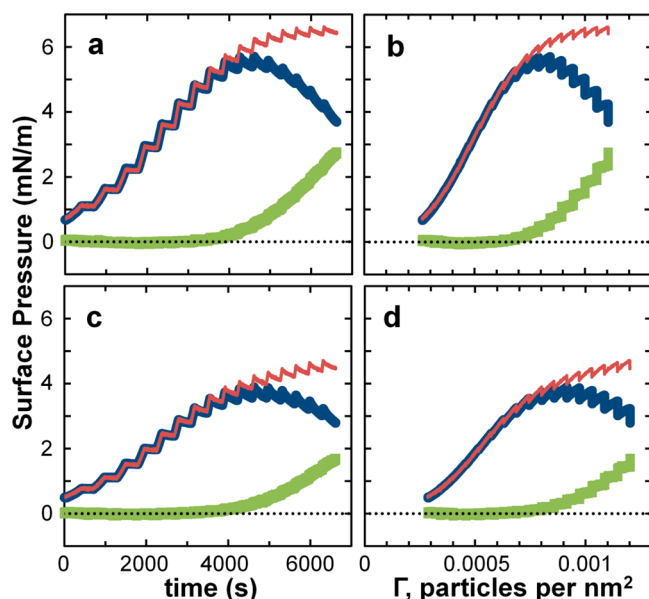


**Figure 8.** Stepped-compression experiments, designed to minimize inaccuracies caused by delays in adsorption/desorption due to desorption kinetics and mass transport. The surface is compressed at a rate of  $4.5 \text{ cm}^2/\text{min}$  in increments of  $\Delta\Gamma/\Gamma_0 = 0.2$ , with each incremental compression followed by a 5 min period where the area is held fixed, to allow the monolayer to relax. Surface pressures ( $\Pi$ ) plotted as a function of time (a, c) and concentration (b, d) of nanoparticles: (a, b) L5 and (c, d) L2.5 reveal NP desorption energies more accurately than continuous compression. Symbols as in Figure 7.

Assuming the surface to be hexagonally close-packed, the characteristic interparticle separation at the onset of desorption can be estimated from the critical surface concentration,  $\Gamma_{\text{des}}$ , via

$$S_{\text{des,hcp}} = 2 \sqrt{\frac{0.91}{\pi\Gamma_{\text{des}}}} \quad (3)$$

The separation distance of the nanoparticles measured at air–water surfaces (calculated using eq 3 to be 39.7 and 37.3 nm for L5 and L2.5, respectively) and at the decane–water interface (measured using X-ray reflectivity<sup>15</sup> at saturation to be 54.4 and 39.8 nm for L5 and L2.5, respectively) are both significantly larger than the diameter of nanoparticles in bulk aqueous solution (measured to be 30 and 23 nm for L5 and L2.5, respectively).<sup>15</sup> This large lattice spacing indicates PEO-functionalized NPs interact repulsively over distances longer than the equilibrium brush thickness in bulk solution, revealing instead the PEO corona around each interfacially adsorbed NP to be strongly deformed and highly flattened (e.g., Figure 9). Similar morphologies have been directly observed for larger soft

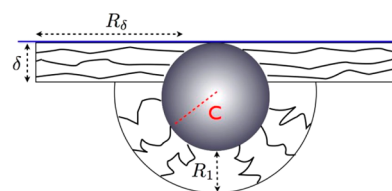


**Figure 9.** Schematic of a simple model used to compute the free energy of adsorption of core–shell (iron oxide–PEO) nanoparticles at the air–water interface. The model accounts for an interfacial layer of thickness  $\delta$  and length  $R_\delta$  of strongly deformed PEO chains, adsorbed onto a particle core of radius  $C$ . Fully submerged polymer chains, with homogeneous grafting density  $\Sigma$ , form a brush of thickness  $R_1$ .

particles.<sup>40</sup> The desorption processes measured here thus involve the interaction of significantly stretched interfacial shells. As with homopolymer chains, entire NPs desorb from the particulate monolayer once further compression of interfacial PEO chains/shells would cost more energy than expelling a particle from the interface.

During adsorptive equilibration, nanoparticles adsorb to the interface until the energy required to make sufficient space for the adsorption of an additional particle is higher than the energy gained from the particle adsorption. Detailed balance, of course, dictates that adsorption and desorption rates be equal in equilibrium. In equilibrium, then, desorption pressures and concentrations  $\Pi_{\text{des}}$  and  $\Gamma_{\text{des}}$  must be identical to the analogous quantities measured during spontaneous adsorption measurements. Various dynamical processes are required to achieve equilibrium, however, and extremely slow kinetics may render equilibration times prohibitively long. Nonetheless, the desorption surface pressures measured in stepped-compression experiments are very close to those measured via spontaneous adsorption (as reported in Figure 7c). Furthermore, the lattice spacing inferred from desorption measurements on air–water interfaces ( $S_{\text{des,hcp}} \sim 40 \text{ nm}$ ) agrees well with lattice spacings measured at decane–water interfaces using X-ray reflectivity.<sup>15</sup> These results highlight that the size of the stretched PEO shell depends only weakly on the nature of the nonpolar phase.

Previous calculations of the adsorption energy of core–shell PEO–iron oxide NPs at the oil/water interface<sup>14</sup> considered the different solubility of the PEO chains in the two solvents but neglected the effects of the interface. Reasonable estimates were nonetheless obtained for  $\Delta E_{\text{ADS}}$ . The experiments presented here, however, strongly suggest the PEO shells are highly deformed at the interface and that a more accurate model must account for the effects of the interface itself. We have thus incorporated interfacial deformations into a simple model system, shown in Figure 9, which we now use to calculate the free energy of adsorption of PEO NPs at the air–water interface.

**Table 1. Nanoparticle Adsorption Parameters<sup>a</sup>**

particle	$\Gamma_{\text{des}}, \text{nm}^{-2}$	$\Pi_{\text{des}}, \text{mN/m}$	$\Delta E, k_B T$	$S_{\text{des,hcp}}, \text{nm}$	$d_{\text{bulk}}, \text{nm}$	$\Pi_{\text{sat,soln(WP)}}, \text{mN/m}$	$\Pi_{\text{sat,INT(MT/WP)}}, \text{mN/m}$
L5	$7.35 \times 10^{-4}$	5.72	$1930 \pm 250$	39.7	30.0	5.7	6.4
L2.5	$8.35 \times 10^{-4}$	3.92	$1160 \pm 110$	37.3	23.0	3.6	3.0

<sup>a</sup>Nanoparticle adsorption energies ( $\Delta E$ ) are calculated from the critical surface pressure ( $\Pi_{\text{des}}$ ) and concentration ( $\Gamma_{\text{des}}$ ) at desorption from stepped-compression experiments (Figure 7) to be of order  $1000 k_B T$ . The critical desorption pressure ( $\Pi_{\text{des}}$ ) coincides with both the saturation pressure from spontaneous adsorption from bulk solution ( $\Pi_{\text{sat,soln(WP)}}$ ) as well as with the saturation surface pressure of the internal surface ( $\Pi_{\text{sat,INT(MT/WP)}}$ ) due to re-adsorbing nanoparticles in the MT/WP compression experiment. The interparticle separation at desorption ( $S_{\text{des,hcp}}$ ), computed assuming hexagonal close packing, is larger than the effective nanoparticle diameter in aqueous solution ( $d_{\text{bulk}} = 2(r_{\text{core}} + t_{\text{s,bulk}})$ ), including the iron oxide core radius ( $r_{\text{core}} = 8.4 \text{ nm}$ ) and PEO shell thickness ( $t_{\text{s,bulk}} = 10.8$  and  $7.3 \text{ nm}$  for L5 and L2.5, respectively).

We consider first a core–shell nanoparticle fully immersed in a good solvent (water). As in an earlier study,<sup>14</sup> we denote the total number of (homogeneously) grafted chains by  $n = 4\pi C^2/\Sigma$  on the surface of the particle, where  $C$  is the radius of the nanoparticle and  $\Sigma$  the grafting density. The free energy of the polymer-coated nanoparticle can then be written as  $F_1 = n f_1(R_1)$ , where  $f_1(R_1)$  is the free energy of a single chain that is extended to a length  $R_1$ . We further assume that  $f_1$  can be decomposed into an elastic contribution and a mean-field interaction between chains in the brush,  $f_1 = f_1^{\text{elast}} + f_1^{\text{int}}$ . Since air is such a poor solvent compared to water, we assume the nanoparticle resides completely in the good solvent (Figure 9), with grafted polymers stretching out along the interface in a layer of (unknown) thickness  $\delta$ , with the number of chains in this layer given by  $n_\delta = 2\pi C\delta/\Sigma$ . Assuming the rest of the brush to be unperturbed by the interface, the free energy of an adsorbed core–shell nanoparticle can then be written  $F_2 = (n - n_\delta)f_1(R_1) + n_\delta f_\delta(R_\delta)$ , where  $f_\delta$  is the free energy of a single chain in the interface layer and  $R_\delta$  its equilibrium extension. The single-chain free energy is decomposed into different components,  $f_\delta = f_\delta^{\text{elast}} + f_\delta^{\text{int}} + f_{\text{interface}}$ , where  $f_{\text{interface}} = -\gamma_{\text{eff}}N\pi a^2$ ,  $\gamma_{\text{eff}}$  is an effective interfacial tension representing the interaction of EO monomers in the dense, quasi-2D brush with the interface, and  $N$  is the number of monomers of size  $a$  in the layer. Because each monomer gains an amount of  $-\gamma_{\text{eff}}\pi a^2$  when adsorbed to the interface,  $f_{\text{interface}}$  is proportional to  $N$  but independent of the coil size  $R$ . For further details of the model, please see the Supporting Information.

For PEO chains of molecular weight 2737 and 5557 g/mol (chain lengths of  $N = 62$  and  $N = 126$ ) used in this study, we calculate the equilibrium brush height in water to be  $R_1 \approx 5.8$  and 9.0 nm, while the polymer chains in the interface layer are stretched much more significantly, with values of  $R_\delta \approx 13$  and 23 nm, respectively. Precise values for  $R_1$  and  $R_\delta$  are fairly insensitive to the value chosen for the interface layer thickness  $\delta$  within a reasonable range (1–3 nm); those values of  $\delta$  determine an effective 2D grafting density (number of chains per unit length) of the PEO brush confined at the interface which give good agreement with the interparticle separation measured by X-ray reflectivity.<sup>15</sup> Significantly, even this simple model predicts the interface layer to have an extension  $R_\delta$  that compares well with the values deduced from NP desorption measurements.

On the basis of the simple model, we estimate the desorption energy  $\Delta E$  of the coated nanoparticle by the difference in the free energy in the desorbed and adsorbed state,  $\Delta E = F_1 - F_2 = n_\delta[f_1(R_1) - f_\delta(R_\delta)]$ . Thus, the desorption energy is given by the difference in free energy between the chains in the brush (bulk) and in the interface layer. While our model assumes the size of the polymer shell to be independent of the interfacial tension, the desorption energy it predicts scales linearly with  $\gamma_{\text{eff}}$ . Taking a reasonable value of  $\delta = 3$  nm for the interfacial layer thickness, this model predicts the experimentally measured desorption energies with effective interfacial tensions of  $\gamma_{\text{eff}} \approx 21.5$  and 18.5 mN/m for the shorter and longer PEO chains, respectively. Both values of the effective interfacial tension are nearly constant at around  $\gamma_{\text{eff}} \approx 20$  mN/m, irrespective of the PEO chain size.

## CONCLUSION

We have demonstrated a technique to measure the adsorption energy of surface-active polymers and nanoparticles. Using a Langmuir trough to control directly the surface concentration,

we measure the surface pressure with a standard Wilhelmy plate tensiometer and our in-plane, deflection microtensiometer. Deviations in the measured compression isotherms reflect a nonzero surface pressure inside the MT, which arises when polymer and nanoparticle surfactants desorb from the exterior (high-concentration) interface and adsorb onto the (clean or low-concentration) interface interior to the MT. Measurements of the critical surface pressure and concentration required for desorption enables the free energy of adsorption/desorption to be extracted quantitatively.

A PS–PEO block copolymer was shown to aggregate effectively into surface micelles that anchor so strongly to the air–water interface that we never detected desorption. By contrast, PEO homopolymers are surface-active on aqueous interfaces but do desorb from the surface at sufficiently high surface concentrations. The measured adsorption energy per chain scales linearly with the molecular weight of PEO and also depends on the solvent conditions of the subphase.

Iron oxide–PEO core–shell nanoparticles have adsorption energies on the order of  $1000 k_B T$ , in accordance with predictions from a model that takes into account explicitly the surface activity of the PEO chains. The critical surface concentration of desorption is relatively low, supporting a picture of particles that adopt a highly deformed configuration on the surface, with highly stretched PEO ligands. The adsorption pressure, as measured with the comparative MT/WP technique, shows good agreement with WP measurements of spontaneous adsorption from solution. Desorption energies, concentrations, and pressures derived from forced desorption experiments also agree.

Although it may seem reasonable to consider surface-active particles with  $\sim 10^3 k_B T$  desorption energies to be irreversibly adsorbed, sufficiently high pressures can be easily accessed by compression in a Langmuir trough. This result has direct relevance for material fabrication—e.g., for Langmuir–Blodgett deposition of monolayers—and highlights an important, yet generally overlooked feature in the processing of Pickering emulsions stabilized by small nanoparticles. In essence,  $10^3 k_B T$  binding energies may not necessarily be irreversible when interfaces are compressed, and droplets in relative motion may drive localized compressions, causing particle desorption and subsequent destabilization.

Finally, we remark that the adsorption energy of an isolated particle or chain may be different from the desorption energy of the same object from a densely packed monolayer. We expect this to be true for soft and interacting objects, highlighting qualitative differences in adsorption for this more general class of systems, when compared with the special case of hard particles. Our experiments therefore open the way toward the characterization of the adsorption of complex objects at fluid interfaces, with direct relevance for various systems of both fundamental and applied interest.

## ASSOCIATED CONTENT

### Supporting Information

Microtensiometer video (played 60× real time) from Figure 4b demonstrating desorption and readsorption of 3.35K PEO as the external interface is compressed, held at fixed area, expanded, and then the inner interface aspirated; details of the model of nanoparticles at air–water surface. This material is available free of charge via the Internet at <http://pubs.acs.org>.



## AUTHOR INFORMATION

### Corresponding Author

\*E-mail: lucio.isa@mat.ethz.ch (L.I.).

### Notes

The authors declare no competing financial interest.

## ACKNOWLEDGMENTS

This work was supported by the National Science Foundation under Grant CBET-932259, which Z.Z., T.M.S., and L.G.L. gratefully acknowledge. L.I. acknowledges financial support from the Swiss National Science Foundation Grants PP00P2\_144646/1, PZ00P2\_142532/1, and IZKOZ2\_142110/1. We gratefully acknowledge N. Lynd and C. Hawker, who provided the PS-PEO block copolymer samples, and T. Gillich, who provided the core-shell nanoparticles. Work was performed in UCSB's Materials Research Laboratory Central Facilities, which are supported by the NSF MRSEC Program under Grant DMR05-20415, a member of the NSF-funded Materials Research Facilities Network, and in the UCSB nanofabrication facility, part of the NSF-funded NNIN network.

## REFERENCES

- (1) Hamley, I. W. Nanostructure fabrication using block copolymers. *Nanotechnology* **2003**, *14* (10), R39–R54.
- (2) Mendes, P. M.; Preece, J. A. Precision chemical engineering: integrating nanolithography and nanoassembly. *Curr. Opin. Colloid Interface Sci.* **2004**, *9* (3–4), 236–248.
- (3) Li, M.; Coenjarts, C. A.; Ober, C. K. Patternable block copolymers. In *Block Copolymers II*; Abetz, V., Ed.; Springer: Berlin, 2005; Vol. 190, pp 183–226.
- (4) Albrecht, K.; Mourran, A.; Moeller, M. Surface micelles and surface-induced nanopatterns formed by block copolymers. In *Ordered Polymeric Nanostructures at Surfaces*; Vancso, G. J., Ed.; Springer: Berlin, 2006; Vol. 200, pp 57–70.
- (5) Marencic, A. P.; Register, R. A. Controlling order in block copolymer thin films for nanopatterning applications. *Annu. Rev. Chem. Biomol. Eng.* **2010**, *1* (1), 277–297.
- (6) Zhao, L.; Lin, Z. Self-assembly of non-linear polymers at the air/water interface: the effect of molecular architecture. *Soft Matter* **2011**, *7* (22), 10520–10535.
- (7) Boker, A.; He, J.; Emrick, T.; Russell, T. P. Self-assembly of nanoparticles at interfaces. *Soft Matter* **2007**, *3* (10), 1231–1248.
- (8) Garbin, V.; Crocker, J. C.; Stebe, K. J. Nanoparticles at fluid interfaces: Exploiting capping ligands to control adsorption, stability and dynamics. *J. Colloid Interface Sci.* **2012**, *387* (1), 1–11.
- (9) Duan, H.; Wang, D.; Sobal, N. S.; Giersig, M.; Kurth, D. G.; Möhwald, H. Magnetic colloidosomes derived from nanoparticle interfacial self-assembly. *Nano Lett.* **2005**, *5* (5), 949–952.
- (10) Arumugam, P.; Patra, D.; Samanta, B.; Agasti, S. S.; Subramani, C.; Rotello, V. M. Self-assembly and cross-linking of FePt nanoparticles at planar and colloidal liquid-liquid interfaces. *J. Am. Chem. Soc.* **2008**, *130* (31), 10046–10047.
- (11) Tangirala, R.; Hu, Y.; Joralemon, M.; Zhang, Q.; He, J.; Russell, T. P.; Emrick, T. Connecting quantum dots and bionanoparticles in hybrid nanoscale ultra-thin films. *Soft Matter* **2009**, *5* (5), 1048–1054.
- (12) Pieranski, P. Two-dimensional interfacial colloidal crystals. *Phys. Rev. Lett.* **1980**, *45* (7), 569–572.
- (13) Du, K.; Glogowski, E.; Emrick, T.; Russell, T. P.; Dinsmore, A. D. Adsorption energy of nano- and microparticles at liquid-liquid interfaces. *Langmuir* **2010**, *26* (15), 12518–12522.
- (14) Isa, L.; Amstad, E.; Schwenke, K.; Del Gado, E.; Ilg, P.; Kroger, M.; Reimhult, E. Adsorption of core-shell nanoparticles at liquid-liquid interfaces. *Soft Matter* **2011**, *7* (17), 7663–7675.
- (15) Isa, L.; Calzolari, D. C. E.; Pontoni, D.; Gillich, T.; Nelson, A.; Zirbs, R.; Sanchez-Ferrer, A.; Mezzenga, R.; Reimhult, E. Core-shell nanoparticle monolayers at planar liquid-liquid interfaces: effects of polymer architecture on the interface microstructure. *Soft Matter* **2013**, *9* (14), 3789–3797.
- (16) Calzolari, D. C. E.; Pontoni, D.; Deutsch, M.; Reichert, H.; Daillant, J. Nanoscale structure of surfactant-induced nanoparticle monolayers at the oil-water interface. *Soft Matter* **2012**, *8* (45), 11478–11483.
- (17) Gillich, T.; Acikgöz, C.; Isa, L.; Schlüter, A. D.; Spencer, N. D.; Textor, M. PEG-stabilized core-shell nanoparticles: Impact of linear versus dendritic polymer shell architecture on colloidal properties and the reversibility of temperature-induced aggregation. *ACS Nano* **2013**, *7* (1), 316–329.
- (18) Zell, Z. A.; Choi, S. Q.; Leal, L. G.; Squires, T. M. Microfabricated deflection tensiometers for insoluble surfactants. *Appl. Phys. Lett.* **2010**, *97* (13), 133505–3.
- (19) Bijsterbosch, H. D.; de Haan, V. O.; de Graaf, A. W.; Mellema, M.; Leermakers, F. A. M.; Cohen Stuart, M. A.; van Well, A. A. Tethered adsorbing chains: Neutron reflectivity and surface pressure of spread diblock copolymer monolayers. *Langmuir* **1995**, *11* (11), 4467–4473.
- (20) Gonçalves da Silva, A. M.; Filipe, E. J. M.; d'Oliveira, J. M. R.; Martinho, J. M. G. Interfacial behavior of poly(styrene)-poly(ethylene oxide) diblock copolymer monolayers at the air-water interface. Hydrophilic block chain length and temperature influence. *Langmuir* **1996**, *12* (26), 6547–6553.
- (21) Fauré, M. C.; Bassereau, P.; Carignano, M. A.; Szeleifer, I.; Gallot, Y.; Andelman, D. Monolayers of diblock copolymer at the air-water interface: the attractive monomer-surface case. *Eur. Phys. J. B* **1998**, *3* (3), 365–375.
- (22) Cox, J. K.; Yu, K.; Constantine, B.; Eisenberg, A.; Lennox, R. B. Polystyrene-poly(ethylene oxide) diblock copolymers form well-defined surface aggregates at the air/water interface. *Langmuir* **1999**, *15* (22), 7714–7718.
- (23) Cox, J. K.; Yu, K.; Eisenberg, A.; Lennox, R. B. Compression of polystyrene-poly(ethylene oxide) surface aggregates at the air/water interface. *Phys. Chem. Chem. Phys.* **1999**, *1* (18), 4417–4421.
- (24) Baker, S. M.; Leach, K. A.; Devereaux, C. E.; Gragson, D. E. Controlled patterning of diblock copolymers by monolayer Langmuir-Blodgett deposition. *Macromolecules* **2000**, *33* (15), 5432–5436.
- (25) Kim, Y.; Pyun, J.; Fréchet, J. M. J.; Hawker, C. J.; Frank, C. W. The dramatic effect of architecture on the self-assembly of block copolymers at interfaces. *Langmuir* **2005**, *21* (23), 10444–10458.
- (26) Shuler, R. L.; Zisman, W. A. Study of the behavior of polyoxyethylene at the air-water interface by wave damping and other methods. *J. Phys. Chem.* **1970**, *74* (7), 1523–1534.
- (27) Kawaguchi, M.; Komatsu, S.; Matsuzumi, M.; Takahashi, A. Concentration dependence of surface pressure of polyether monolayers at the air-water interface. *J. Colloid Interface Sci.* **1984**, *102* (2), 356–360.
- (28) Sauer, B. B.; Kawaguchi, M.; Yu, H. A surface light scattering study of poly(ethylene oxide) and poly(vinyl acetate) at the air/water and heptane/water interfaces. *Macromolecules* **1987**, *20* (11), 2732–2739.
- (29) Kuzmenka, D. J.; Granick, S. Collapse of poly(ethylene oxide) monolayers. *Macromolecules* **1988**, *21* (3), 779–782.
- (30) Sauer, B. B.; Yu, H. Adsorption kinetics of poly(ethylene oxide) at the air/water interface. *Macromolecules* **1989**, *22* (2), 786–791.
- (31) Sauer, B. B.; Yu, H.; Yazdani, M.; Zografi, G.; Kim, M. W. An ellipsometric study of polymer monolayers at the air/water interface. *Macromolecules* **1989**, *22* (5), 2332–2337.
- (32) Holland, N. B.; Xu, Z.; Vacheethasane, K.; Marchant, R. E. Structure of poly(ethylene oxide) surfactant polymers at air-water and solid-water interfaces. *Macromolecules* **2001**, *34* (18), 6424–6430.
- (33) Xu, Z.; Holland, N. B.; Marchant, R. E. Conformations of short-chain poly(ethylene oxide) lipopolymers at the air-water interface: A combined film balance and surface tension study. *Langmuir* **2000**, *17* (2), 377–383.

- (34) Devanand, K.; Selser, J. C. Asymptotic behavior and long-range interactions in aqueous solutions of poly(ethylene oxide). *Macromolecules* **1991**, *24* (22), 5943–5947.
- (35) Kent, M. S.; Lee, L. T.; Factor, B. J.; Rondelez, F.; Smith, G. S. Tethered chains in good solvent conditions: An experimental study involving Langmuir diblock copolymer monolayers. *J. Chem. Phys.* **1995**, *103* (6), 2320–2342.
- (36) Rubin, R. J. Random-walk model of chain-polymer adsorption at a surface. *J. Chem. Phys.* **1965**, *43* (7), 2392–2407.
- (37) Tsierkezos, N. G.; Molinou, I. E. Thermodynamic properties of water + ethylene glycol at 283.15, 293.15, 303.15, and 313.15 K. *J. Chem. Eng. Data* **1998**, *43* (6), 989–993.
- (38) Garbin, V.; Crocker, J. C.; Stebe, K. J. Forced desorption of nanoparticles from an oil-water interface. *Langmuir* **2012**, *28* (3), 1663–1667.
- (39) Stefaniu, C.; Chanana, M.; Wang, D.; Novikov, D. V.; Brezesinski, G.; Möhwald, H. Biocompatible magnetite nanoparticles trapped at the air/water interface. *ChemPhysChem* **2010**, *11* (17), 3585–3588.
- (40) Geisel, K.; Isa, L.; Richtering, W. Unraveling the 3D localization and deformation of responsive microgels at oil/water interfaces: A step forward in understanding soft emulsion stabilizers. *Langmuir* **2012**, *28* (45), 15770–15776.